Nonlinear looped band structure of Bose-Einstein condensates in an optical lattice

S. B. Koller, E. A. Goldschmidt, R. C. Brown, R. Wyllie, R. M. Wilson, and J. V. Porto

Phys. Rev. A **94**, 063634 — Published 23 December 2016

DOI: 10.1103/PhysRevA.94.063634

Nonlinear looped band structure of Bose-Einstein condensates in an optical lattice

S. B. Koller,[1,2] E. A. Goldschmidt,[3] R. C. Brown,[1,*] R. Wyllie,[1,†] R. M. Wilson,[4] and J. V. Porto[1]

[1] *Joint Quantum Institute, National Institute of Standards and Technology and University of Maryland, Gaithersburg, Maryland 20899, USA*
[2] *Physikalisch-Technische Bundesanstalt, Braunschweig, Germany*
[3] *United States Army Research Laboratory, Adelphi, Maryland 20783, USA*
[4] *Department of Physics, United States Naval Academy, Annapolis, Maryland 21402, USA*

(Dated: November 22, 2016)

We study experimentally the stability of excited, interacting states of bosons in a double-well optical lattice in regimes where the nonlinear interactions are expected to induce "swallowtail" looped band structure. A dynamic homogeneous Gross-Pitaevskii calculation indicates that the double well lattice both stabilizes the looped band structure and allows for dynamic preparation of different initial states, including states within the loop structure. The homogeneous calculation predicts that the loop states, unlike the ground states, should be dynamically stable. An inhomogeneous mean-field calculation including the trap potential, however, implies that the decay is dominated by inhomogeneous effects and that there is little variation in the decay rate among the states prepared within the loop structure. By experimentally preparing different initial coherent states and observing their subsequent decay, we observe distinct decay rates in regimes where multi-valued looped band structure is expected, though not the stability predicted by the homogeneous calculation.

Interactions in Bose-Einstein condensates (BECs) can give rise to qualitatively new nonlinear phenomena [1–5]. For example, superfluids in optical lattices can exhibit additional, interaction-stabilized states arising from the so-called "swallowtail catastrophe" in which the band structure becomes multi-valued [6–9]. As the interaction increases, the collective band structure at the edge of the Brilloiun zone (BZ) develops a cusp (a discontinuity in the derivative), and subsequently a loop with multiple energy states that can be occupied at the same quasimomentum. The existence of loop states is related to dynamical asymmetry in Landau-Zener tunneling between coupled states of the many-body system [10], which has been used to indirectly observe nonlinear loop structure [4, 11]. Despite the fact that ultracold atoms in optical lattices are an ideal system to realize nonlinear wave dynamics, the interaction strengths needed to generate such interesting band structure in a single-period square lattice are prohibitively large for ultracold atom systems.

In addition to multi-valued band structure at the edge of the BZ, period doubled solutions are also expected to occur halfway to the edge of the BZ [12]. Adding a weak lattice at half the main lattice period expands the parameter regime where band structure loops are expected [8], making them more experimentally feasible. The states associated with the loop are collective excited states, and an essential consideration in their observation is their stability [13–17]. Even in the weakly interacting, mean-field limit, dynamical instabilities can arise that quickly destroy the excited superfluid state [18–20]. However, dynamically stable mean-field solutions exist [21], and there are experimentally accessible regimes where mean-field calculations predict different decay rates for the multi-valued bands. Notably, a homogeneous mean-field theory predicts a regime where excited loop states are dynamically stable near the band edge, while states in the ground band are dynamically unstable. An example of such looped band structure is shown by the grey line in Fig. 1a.

Here, we dynamically produce nonlinear excited states of a harmonically trapped BEC in a two dimensional checkerboard optical lattice and show experimentally that, depending on which initial nonlinear state is prepared, the subsequent dynamics is multi-valued in parameter regimes where loop states are expected. In particular, we observe distinct decay rates near the band edge in the presence of a weak lattice at half the main lattice period. In this way, our observations are in qualitative agreement with a homogeneous mean-field theory. However, we observe a substantial decay in the loop states that is not captured by this theory, indicating that inhomogeneities and correlations that invalidate this mean-field description may play an important role [22]. While an inhomogeneous mean-field theory that includes the harmonic trapping potential exhibits this decay, it otherwise does not provide an accurate description of the experimental data. However, we note that beyond mean-field correlations can cause additional instabilities in the excited states [4, 22], and may play a role in this system. Finally, by measuring the energy released upon decay, we show that there is an energy difference between the different state preparations, providing additional evidence of multi-valued band structure.

Although homogeneous mean-field calculations predict the existence of stable loop states at the band edge, such states are not necessarily trivial to produce experimentally. The mean-field interacting states obey Bloch's equation and are characterized by a quasimomentum q.

* Current address: National Institute of Standards and Technology, Boulder, Colorado 80305 USA
† Current address: Quantum Systems Division, Georgia Tech Research Institute, Atlanta, Georgia 30332, USA

Raman or Bragg excitation can excite weakly-interacting BECs to a given quasimomentum $q \neq 0$ because the initial and final states are single-particle in nature, as are such excitation techniques. The loop states, however, rely on interactions, and it is not clear how well single-particle Raman excitation couples to such collective states via intermediate states with only partial transfer. In order to prepare states in the interacting band, we use a combination of adiabatic and diabatic manipulation of the lattice structure [16, 23] while accelerating the BEC to momenta near the band edge.

The 2D lattice is produced with a 813 nm laser in a bow-tie configuration in the xy-plane and weak harmonic confinement in the z-direction, giving rise to a checkerboard array of 1D tubes with ~ 100 atoms per tube at the center of the cloud [24]. The staggered energy offset, Δ, between neighboring tubes can be dynamically controlled on timescales as short as 10 μs, much faster than any dynamic timescale in the system. For $\Delta \neq 0$, the fundamental lattice period increases from the usual $\lambda/2$ to $\lambda/\sqrt{2}$, and the Bravais lattice and associated BZ are rotated 45 degrees with respect to the original $\lambda/2$ lattice (Fig. 1c). A stable looped structure is expected along the edge of the smaller BZ for Δ on the order of interaction energy parameterized by $g\bar{n}$ ($\bar{n}$ is the average atomic density [25] and $g = 4\pi\hbar^2 a/m$, where a is the scattering length and m the mass of ^{87}Rb). We develop three different procedures (described below), to prepare initial states that we label "(G)round", "(E)xcited" and "(L)oop" and then study the stability of each of these states by measuring characteristic decay timescales as functions of quasimomentum q, staggered offset Δ, and atomic density n.

All experiments start with a ^{87}Rb BEC at rest ($q = 0$) in the ground band of a $V_{\rm lat} = 10.6\,E_R$ lattice with a staggered offset too large to support a loop. (Here, $E_R = \hbar k_R^2/2m = 3.5$ kHz is the single-photon recoil energy associated with the short period lattice, $k_R = 2\pi/\lambda = \sqrt{2}k_X$.) A force, F, is applied to the atoms using a magnetic field gradient, resulting in an acceleration $\dot{q} = F$ along the direction "X" associated with the long period of the lattice (see Fig. 1) to near the edge of the band, which occurs at $q = k_X = \pi/(\lambda/\sqrt{2})$. The force is chosen to accelerate fast enough to minimize the decay associated with dynamic instabilities [20], yet slow enough to preclude band excitation. The resulting acceleration rate is calibrated by pulling the atoms through the entire BZ and observing Bloch oscillations of q [26]. The angle between the force and the X direction of the BZ was determined to be less than 0.4 degrees by comparing Bloch oscillation patterns to atom diffraction after pulsing the lattice.

For each state preparation sequence, G, L, and E, the final lattice configuration is identical, with a final staggered offset Δ of order the interaction energy $g\bar{n}$. For the G sequence, the accelerating force is applied until the desired final q is reached, at which point the offset is reduced (in 50 μs) to the final value Δ. For the L and

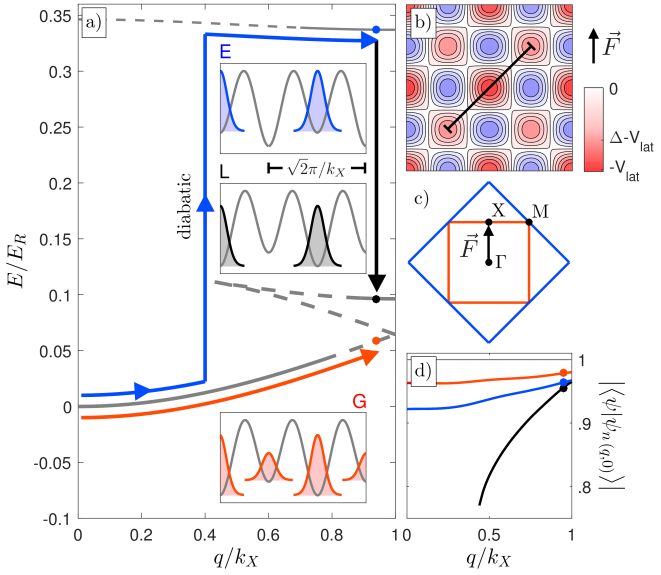

FIG. 1. (a) State preparation of an interacting BEC in the looped band structure (grey solid and dashed lines). Dashed parts of the band structure indicate dynamically unstable regions. A combination of forces to accelerate the quasimomentum and control of the staggered offset Δ are used to prepare the BEC in the ground (red), loop (black), or excited (blue) bands as indicated schematically by the lines with arrows and described in the text. Note that until the final state preparation step, the staggered offset is too large to support a loop. The insets show the final wavefunctions calculated by a time-dependent Gross-Pitaevskii (GP) simulation. (b) Real-space lattice potential with staggered wells in 2D. (c) 2D Brillouin zones associated with the lattice of period $\lambda/2$ (blue) and $\lambda/\sqrt{2}$ (red). Acceleration is from $q = 0$ at Γ to $q = k_X$ at X. (d) Overlap between the dynamic GP simulation and the ideal wavefunctions for the E, L, and G preparations sequences, as a function of q.

E sequences, when the accelerating force brings the BEC to $q \approx k_X/2$, the sign of the staggered offset is switched (in 50 μs), projecting the state into the excited band. Switching at $q \approx k_X/2$ avoids the most unstable regions $0 < q < k_X/2$ in the excited band and $k_X/2 < q < k_X$ in the ground band. The accelerating force continues to increase q with the BEC in the excited band until the desired q is reached, at which time the offset is switched to the final Δ and the accelerating force is terminated. The wavefunctions in the excited and loop bands are nearly identical for $\Delta \to -\Delta$ when q is near k_X so the sign of the final Δ determines whether the E or L state is prepared. See the Appendix for further information on the state preparation.

To characterize the preparation sequences, we simulated the dynamics using the time-dependent Gross-Pitaevskii (GP) equation in a homogeneous system with the time sequences used in the experiment, starting with the GP ground state at $q = 0$. We then calculated the overlap of the dynamically created nonlinear wavefunctions, ψ, with the solutions of the stationary GP equa-

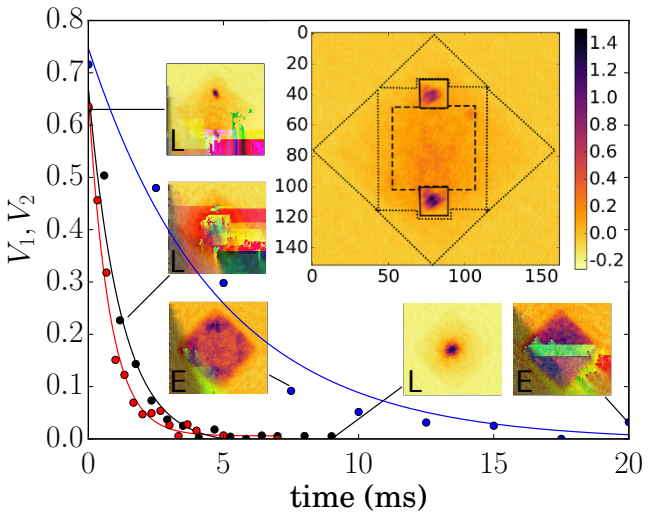

FIG. 2. Decay of visibility as a function of hold time for states prepared by the (G)round (red), (L)oop (black), and (E)xcited (blue) sequences. The examples here correspond to the case of $q = k_X$, Δ/h=0.7 kHz and $g\bar{n}/h$=0.31(1) kHz. The fitted rates for the G-, L-, and E-preparations are 1.29(9) ms^{-1}, 0.84(8) ms^{-1}, and 0.21(3) ms^{-1}, respectively. Large inset: absorption image with analysis regions S (solid lined squares), B_1 (dashed line central square), and B_2 (dotted lined triangles) [25]. Smaller insets: absorption images at different decay times, as indicated.

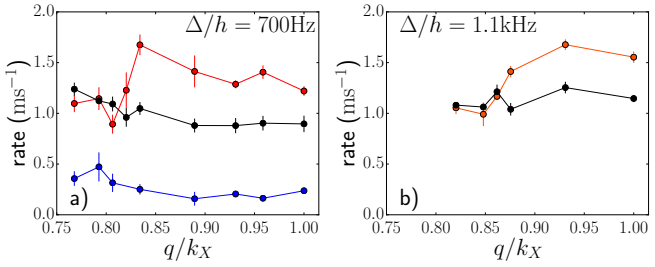

FIG. 3. Measured decay rates vs quasimomentum q of the G (red, light grey), L (black), and E (blue, dark grey) states for a) Δ/h=0.7 kHz and and $g\bar{n}/h$=0.31(1) kHz and b) Δ/h=1.1 kHz and $g\bar{n}/h$=0.29(1) kHz. The color scheme for the G (red), L (black) and E (blue) prepared states is the same as in Fig. 2 and error bars indicate the standard deviation from the exponential fit.

tion, ψ_{nq} where n = G, L, E is the band index, at the same q and Δ. The resulting overlap with the given target state is better than 90% for the range of q studied for all three sequences, as shown by the solid lines in Fig. 1d. Note that unlike for linear equations, two different nonlinear solutions to the same GP equation are not expected to be orthogonal, and overlap with the unwanted states does not imply preparation infidelity. Indeed, there is significant overlap between the different solutions of the stationary GP equation. We note that non-adiabatic excitation of the states, in addition to inhomogeneity, can contribute to the instability of dynamically prepared states.

Having prepared states near the desired state in a given lattice configuration, the BEC is held in the lattice for a variable time t_D. The lattice is subsequently turned off in 1.5 ms, chosen such that the quasimomentum distribution is mapped to position following time-of-flight [25]. We take an absorption image and determine the occupation of the first and second BZ for each preparation sequence and t_D. To quantify the decay, the absorption signal is integrated over regions of the BZ that contain the initial coherent BEC to get the average column density S within those small regions. The signal S is compared to the integrated column density B_1 (B_2) contained in the first (second) BZ, with visibility defined as [25]

$$V_i = \frac{S - B_i}{S + B_i} + C, \qquad (1)$$

where C is chosen so that the visibility V_i decays to zero. The observed relaxation of V_i is approximately exponential, so to characterize the decay timescale we fit it to an exponential function. Example V_i are shown in Fig. 2, with example images of the filling of the first and second BZ as insets. The large inset indicates the regions S, B_1, and B_2.

The behavior of the decay is qualitatively and quantitatively different for the different preparation sequences: the E sequence leads to slower decay (near the band edge) that initially fills the second BZ before eventually filling the first BZ, while the G and L sequences lead to decay that initially fills the first BZ. (For the G and L sequences, the relatively small total energy available within the ground band can relax into the direction perpendicular to the lattice, resulting in a narrowing of the momentum distribution around q=0 in the 2D plane at long times [16]. In contrast, the much larger energy associated with the gap to the excited band results in significantly more heating within the 2D plane after decay.) V_1 is used to extract decay rates for the G and L preparations and V_2 is used to extract a decay rate for the E prepared states. Despite the fact that the final lattice configurations are identical for the G and L sequence, we find that the L prepared states decay more slowly than the G states over a range of parameters.

We first study the stability of the G, L, and E states as a function of quasimomentum q. Fig. 3 shows the decay rates for the ground and loop states for two different staggered offsets $\Delta/h = 0.7$ kHz, 1.1 kHz and similar interaction energy $g\bar{n}/h \approx 0.31$ kHz. The slower, excited band decay (in blue) is shown primarily for reference when included. We find the L decay rate is approximately 40% smaller than the G decay rate for q near the band edge, indicating greater stability of the loop states in that region. The discrepancy in decay rate disappears, however, at smaller q. The closing of the discrepancy between the L and G decay rates occurs at larger q for larger staggered offset Δ. This is the same behavior predicted by the homogeneous mean-field theory for the loop closure

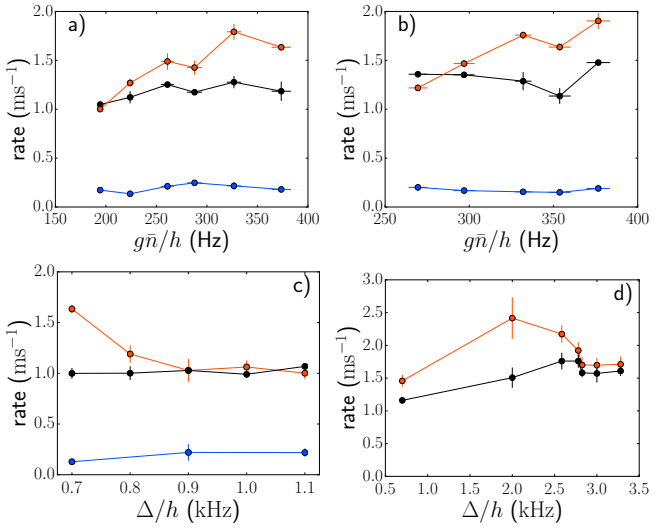

FIG. 4. Decay rates vs interaction energy $g\bar{n}$ for different states G (red, light grey), L (black), E (blue, dark grey) with $q = k_X$ and a) Δ/h=0.9 kHz and b) Δ/h=1.1 kHz. Decay rates vs offset Δ/h with c) $q = 0.82\ k_X$ and $g\bar{n}/h = 0.29(1)$ kHz and d) $q = k_X$ and $g\bar{n}/h = 0.4(2)$ kHz. Vertical error bars indicate the standard deviation from the fit of the decay and horizontal error bars on a) and b) indicate the standard deviation of the mean of all measured instances.

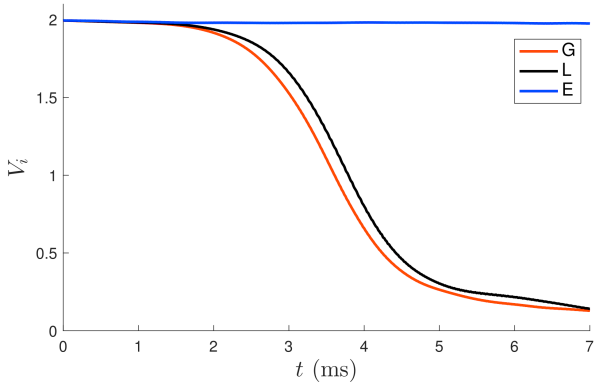

FIG. 5. Simulated visibility V_i (defined in text) as a function of time for states prepared by the (G)round (red, light grey), (L)oop (black), and (E)xcited (blue, dark grey) sequences to $q = k_X$ for a temperature $T = 50$ nK. in an inhomogeneous lattice. These simulations show faster decay of the G and L states, and a more stable E state, consistent with the experimental observations, and were produced with an inhomogeneous 2D GP calculation (details in Appendix).

point (see [21] and the Appendix).

The homogeneous mean-field theory also predicts a critical value of the offset Δ for a given interaction energy $g\bar{n}$, above which no loop is present, and this value of Δ is predicted to increase with increasing $g\bar{n}$. We thus expect the loop to only be present for a value of Δ that is set by the interaction energy. We observe this behavior, as the difference between the L and G decay rates decreases for increasing Δ or decreasing atomic density (see Fig. 4). In particular, the interaction necessary to observe a difference between the G and L state is higher for larger staggered offset, as seen in Fig. 4a-b. In addition, Fig. 4c-d shows that the loop and ground decay rates converge closer to the band edge for larger staggered offset, as in Fig. 3.

To understand the effects of the inhomogeneity introduced by the harmonic trap on the dynamics, we performed 2D GP simulations of the state preparation and subsequent dynamics in a regime where the homogeneous mean-field theory predicts a dynamically stable loop near the band edge (see more details in the Appendix). Fig. 5 shows V_i as extracted from these simulations for $g\bar{n}/h = 0.31$ kHz and the target states at $q = k_X$. While the decay is not immediately exponential as observed in the experiment, the L state (shown by the black line) does decay on a timescale of a few ms, as observed. The state in the E band (shown by the blue line) is much more stable than the states in the L and the G band, which is consistent with our experimental observations. However, the difference in the decay rates of the G and L states does not agree with our experimental observations, and generally these simulations do not provide accurate agreement with our observations for target states at other values of q. This suggests that beyond mean-field correlations or spatial dynamics in the z-direction are important to fully understand the observed data.

An additional consequence of the nonlinear band structure is that the total energy of the looped band state should be more than the ground band state at the same q. We investigate the energy released from the differently prepared states by measuring the cloud width after decay. For each preparation sequence, we calculate the mean square width of the quasimomentum distribution, $w^2 = \langle r^2 n(r)\rangle / \langle n(r)\rangle$, at times much longer than the decay time, where r is the distance measured from the center of the BZ. As shown in Fig. 6, the loop prepared states have larger final energy than the ground states, despite the fact they have identical lattice configurations and the loop state decays more slowly. The discrepancy in released energy is reduced, but does not vanish, when the decay rate gap closes, perhaps indicating either additional energy due to imperfect state preparation during the L sequence or a region of multi-valued bandstructure in which the loop and ground bands have the same stability. We note that the decay rates and energy released for the three different state preparations trend in opposite directions: the faster decaying G states have smaller final w^2, while the slower L and E states have larger final w^2. This supports a description of decay driven by dynamic instabilities, rather than energetic considerations.

The observed convergence of the decay rate of the G and L prepared states occurs at values of q, Δ, and $g\bar{n}$ that agree qualitatively with the trends we expect from a mean-field calculation. However these points do not agree with a quantitative analysis of the region where

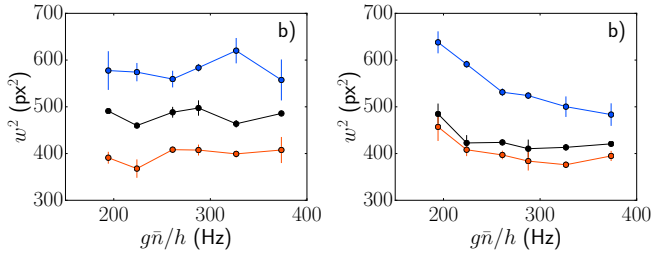

FIG. 6. Mean squared width, w^2, after decay from the Ground (red, light grey), Loop (black) and Excited (blue, dark grey) prepared states, a) as a function of q at an offset of 700 Hz. (Compare with Fig. 3a)), and b) as a function of interaction energy $g\bar{n}/h$ for Δ/h=1.1 kHz. Error bars indicate the standard deviation from different measurements over all states.

a stable loop is predicted given the Bogliubov spectrum either in full 2D or restricted to modes in the direction of the acceleration in quasimomentum [25]. This discrepancy suggests the measured decay rates are due to a combination of effects beyond just the dynamic stability of the mean-field state, including inhomogeneities across the lattice, state preparation infidelities and beyond mean-field correlations. It is clear, however, that the nature of the mean-field state for a given preparation plays an important role in the relaxation. The decay mechanisms and their interplay with the transverse degrees of freedom is an interesting topic that could be further studied by adding a weak lattice in the third spatial dimension to control the magnitude of correlations and dispersion in that direction.

The authors thank M. Foss-Feig for helpful discussions. This work was partially supported by the ARO's Atomtronics MURI. RMW acknowledges partial support from the National Science Foundation under Grant No. PHYS-1516421.

I. APPENDIX

A. Lattice and state preparation

All experiments begin with a ^{87}Rb BEC with no discernible thermal fraction in the $|F = 1, m_F = -1\rangle$ internal hyperfine state, optically trapped with trap frequencies $(\nu_x, \nu_y, \nu_z) = (12(2), 40(4), 100(9))$ Hz. Control of the atom number, independent of trap parameters, is achieved by microwave removal of a fraction of atoms before the final stage of cooling. The lattice depth and offset Δ are determined from an experimentally calibrated model of the 2D lattice potential [24]. We parameterize the interaction energy by $g\bar{n}$, where $\bar{n}$ is the peak density averaged over a unit cell, $\bar{n} = (2/\lambda^2)n_{1D}(z = 0)$ and n_{1D} is the 1D density along the lattice-free central tube. The interaction energy, $g\bar{n}(\lambda^2/2)\int d^2r\,|\phi(\mathbf{r})|^4$, depends on the size of the compressed localized Wannier function $\phi(\mathbf{r})$, ($\phi(\mathbf{r})$ is normalized to 1). For the lattice depths considered here, $(\lambda^2/2)\int d^2r\,|\phi(\mathbf{r})|^4 \simeq 4$, giving rise to an effective factor of four increase in interaction compared to a lattice-free case with the same average density. The value of $g\bar{n}$ is calculated either from an effective Thomas-Fermi approximation using the measured total atom number N and trap frequencies (including the lattice), or from a full 3D ground state solution of the GP equation in the lattice. The two methods agree to 5 %.

The preparation sequences were empirically chosen to optimize the coherence of the final state BEC, while avoiding band excitations and minimizing dynamical instability decay during preparation. The BEC was initially loaded into a 8.9 E_R lattice with positive offset $\Delta_1 > 0$ by turning on the lattice beams during 200 ms, followed by a 400 ms hold time. ($\Delta_1/h = 2.8$ kHz for the E and L sequence and $\Delta_1/h = 1.7$ kHz for the G sequence.) In order to minimize excitations during subsequent lattice manipulations, the lattice depth is then ramped in 0.5 ms to a depth of 10.6 E_R and a larger offset Δ_2. ($\Delta_2/h = 3.3$ kHz for the E and L sequences, and $\Delta_2 = 2.0$ kHz for the G sequence.)

After the increase in lattice depth, a magnetic field gradient is turned on to accelerate the BEC from $q = 0$ to the final value near $q = k_X$ in a time $t_F \simeq 1$ ms. The acceleration time was chosen to prevent excitations, but to minimize dynamical decay during the acceleration. The switch from positive to negative offset in the E and L sequences, as well as the switch to the final offset value, only couple states with the same q, and were chosen to project the BEC onto particular states in the resulting band structure without residual band excitation. The switch from positive to negative offset was tested at $q = 0$ by switching back and looking for excitation in the second BZ. No discernible excited fraction was observed for the lattice depth used. The GP simulations confirm that this combination of adiabatic and diabatic manipulations results in preparation of states with large overlap with the desired final states.

B. Image analysis

The data was taken by absorption imaging the atom cloud after 21 ms time-of-flight, effectively measuring the momentum distribution. The lattice turn-off time of 1.5 ms was chosen to "band map" the quasimomentum distribution $n(q)$ onto the free particle momentum distribution $n(p)$. (Near the band edges, it is impossible to be fully adiabatic, but this does not mix q and only results in some mixing of $n(q)$ at points near the band edges that differ by reciprocal lattice vectors.) For the G and L sequences, some additional coherence decay occurs during the band mapping. The resulting momentum distribution is then divided into several regions S, B_1, B_2 and K. The relative position of B_1, B_2 and K are fixed, but the position of region S depends on q, since the signal in S measures the initially prepared BEC state. The signals

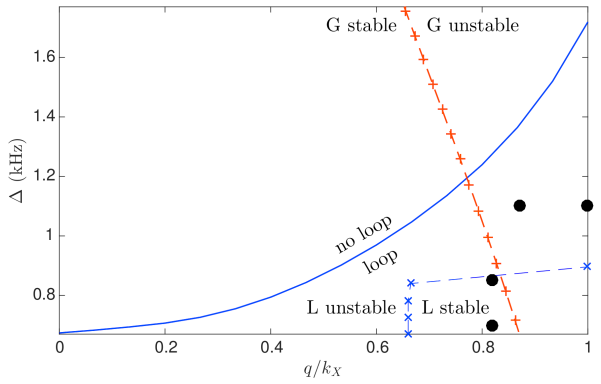

FIG. 7. Presence and stability of the loop band for interaction energy $g\bar{n}/h = 0.31$ kHz as a function of Δ and q in a homogeneous lattice. Multi-valued band structure is present in the region to the right of the solid blue line. The blue dashed line encloses a region where the loop states are dynamically stable. The region to the right of the dashed red line corresponds dynamically unstable states in the ground band.

in regions B_1 and B_2 measure the population outside of S in the first and second BZ, respectively. These regions are chosen slightly smaller than the BZ to avoid ambiguous population mixed between different zones. The large triangles K in the corners of the image are used to determine the background per pixel, K/N_K, assuming it is constant over the image and N_K is the number of background pixels. We calculate the background-subtracted signal for the decay curves:

$$\frac{(S - KN_S/N_K) - (B_i - KN_{B_i}/N_K)}{(S - KN_S/N_K) + (B_i - KN_{B_i}/N_K)} + C,$$

where N_X is the number of pixels in zone X and C is a single constant for each preparation G, E or L, chosen so that the visibility decays to zero.

The mean squared width, $w^2 = \langle r^2 n(r)\rangle / \langle n(r)\rangle$, is calculated from images taken after the atom distribution has relaxed. We note that the band mapping technique modifies the initial energy distribution, and the observed time of flight w^2 does not directly represent the energy distribution in the lattice. Within a band, the measured w^2 is monotonically related to the energy in the band.

C. Mean-field loop and stability regions

We model the experimental state preparation, the nonlinear band structure, and the stability of the states with an effective two-dimensional mean-field theory described by the energy functional

$$E = \int d^2r\, \psi^*(\mathbf{r}) \left(\frac{-\hbar^2}{2m}\nabla^2 + V_{\rm lat}(\mathbf{r}) + \frac{g_{\rm 2D}}{2}|\psi(\mathbf{r})|^2 \right) \psi(\mathbf{r}) \tag{2}$$

and the corresponding time-dependent Gross-Pitaevskii equation

$$i\hbar\partial_t\psi(\mathbf{r}) = \left(\frac{-\hbar^2}{2m}\nabla^2 + V(\mathbf{r}) + g_{\rm 2D}|\psi(\mathbf{r})|^2 \right) \psi(\mathbf{r}), \tag{3}$$

where $V(\mathbf{r})$ is the external potential $g_{\rm 2D} = g\bar{n}\lambda^2/2$ is the effective 2D interaction coupling. For calculations of the nonlinear band structure and the dynamics of state preparation, we consider a homogeneous system with only a lattice,

$$V(\mathbf{r}) = \frac{\Delta}{4}\left(\cos(2k_X x) - \cos(2k_X y)\right) + V_{\rm lat}\cos(2k_X x)\cos(2k_X y), \tag{4}$$

$V_{\rm lat}$ is the lattice depth,

We calculate the nonlinear band structure following the method of [21]. We find the stationary Bloch solutions of Eq. (3), which have the form $\psi_{n\mathbf{q}}(\mathbf{r}) = e^{i\mathbf{q}\cdot\mathbf{r}}u_{n\mathbf{q}}(\mathbf{r})$ where n is the band index and $\mathbf{q}$ is the quasi-momentum in two dimensions. We work in the reciprocal space, and expand $u_{n\mathbf{q}}(\mathbf{r}) = \sum_{\mathbf{k}} c_{n\mathbf{k}} e^{i\mathbf{k}\cdot\mathbf{r}}$. We find $\{c_{n\mathbf{k}}\}$ numerically for all relevant values of n and $\mathbf{q}$, reconstruct $\psi_{n\mathbf{q}}$, then find the energy of the state using Eq. (2). In our dynamical simulations of Eq. (3) to model the state preparation, we consider unit cells of area $\lambda^2/2$ and impose periodic boundary conditions in the phase-gradient of $\psi(\mathbf{r})$.

The expected parameter regime for looped band structure at a representative interaction strength of $g\bar{n} = 0.31$ kHz is shown in Fig. 7. Here, the region to the right of the solid blue line indicates the presence of looped band structure. We calculate decay rates using a linear stability analysis, which in this mean-field framework corresponds to a Bogoliubov treatment. We derive the Bogoliubov equations by substituting $\psi_{n\mathbf{q}}(\mathbf{r}) \to \psi_{n\mathbf{q}}(\mathbf{r}) + \delta\sum_{\mathbf{p}}\left(\mathcal{U}_{n,\mathbf{q}+\mathbf{p}}e^{i(\mathbf{p}\cdot\mathbf{r}-\omega t)} + \mathcal{V}^*_{n,\mathbf{q}-\mathbf{p}}e^{-i(\mathbf{p}\cdot\mathbf{r}-i\omega t)}\right)$ in Eq. (3) and linearizing in δ. We diagonalize these equations to obtain the Bogoliubov spectrum. The imaginary part of this spectrum corresponds to decay of the equilibrium state at the rate $\mathrm{Im}[\omega]$. In Fig. 7, the region enclosed by the blue dashed line indicates a dynamically stable state in the loop, and the region to the right of the red dashed line indicates dynamically unstable ground band states.

We model the inhomogeneous state preparation and the subsequent dynamics using Eq. (3) with both a lattice and a harmonic trap, so

$$V(\mathbf{r}) = \frac{1}{2}m\left(\omega_x^2x^2 + \omega_y^2y^2\right) + \frac{\Delta}{4}\left(\cos(2k_X x) - \cos(2k_X y)\right) + V_{\rm lat}\cos(2k_X x)\cos(2k_X y), \tag{5}$$

where $(\omega_x, \omega_y) = 2\pi(\nu_x, \nu_y)$. We first find the stationary ground state of Eq. (2), ψ_0, using imaginary time evolution. To account for fluctuations due to finite temperature, we seed this state with random noise according to the Truncated Wigner formalism [27]. In particular,

we employ a local density approximation with an initial state is given by

$$\psi(\mathbf{r}) = \psi_0(\mathbf{r}) + \sum_{\mathbf{q}} \left(u_{\mathbf{q}}(\mathbf{r})\beta_{\mathbf{q}} + v^*_{\mathbf{q}}(\mathbf{r})\beta^*_{\mathbf{q}} \right) \qquad (6)$$

where $u_{\mathbf{q}}(\mathbf{r}) = u_{\mathbf{q}}\psi_0(\mathbf{r})$ and $v_{\mathbf{q}}(\mathbf{r}) = v_{\mathbf{q}}\psi_0(\mathbf{r})$, where $u_{\mathbf{q}}$ and $v_{\mathbf{q}}$ are solutions of the Bogoliubov equations for a spatially homogeneous system with $V(\mathbf{r}) = 0$ and BEC density $\bar{n}$, and $\beta_j = \sqrt{n_{\mathbf{q}} + 1/2}\,(x_j + iy_j)/\sqrt{2}$, where x_j and y_j are normally distributed Gaussian random variables with zero mean and unit variance and $n_{\mathbf{q}} = (e^{\omega_{\mathbf{q}}/k_BT} - 1)^{-1}$ is the Bose-Einstein distribution [28]. The sum in Eq. (6) runs over momenta $\mathbf{q}$ such that $q_{\min} < |\mathbf{q}| < q_{\max}$ where $q_{\min}$ is approximately the inverse Thomas-Fermi radius of the cloud, and $q_{\max} = 10k_X$.

[1] J. Denschlag, J. E. Simsarian, D. L. Feder, C. W. Clark, L. A. Collins, J. Cubizolles, L. Deng, E. W. Hagley, K. Helmerson, W. P. Reinhardt, S. L. Rolston, B. I. Schneider, and W. D. Phillips, Science **287**, 97 (2000).

[2] A. Weller, J. P. Ronzheimer, C. Gross, J. Esteve, M. K. Oberthaler, D. J. Frantzeskakis, G. Theocharis, and P. G. Kevrekidis, Physical Review Letters **101**, 130401 (2008).

[3] S. Burger, K. Bongs, S. Dettmer, W. Ertmer, K. Sengstock, A. Sanpera, G. V. Shlyapnikov, and M. Lewenstein, Physical Review Letters **83**, 5198 (1999).

[4] Y.-A. Chen, S. Huber, S. Trotzky, I. Bloch, and E. Altman, Nature Physics **7**, 61 (2011).

[5] L. Deng, E. W. Hagley, J. Wen, M. Trippenbach, Y. Band, P. S. Julienne, J. E. Simsarian, K. Helmerson, S. L. Rolston, and W. D. Phillips, Nature **398**, 218 (1999).

[6] B. Wu and Q. Niu, New Journal of Physics **5**, 104 (2003).

[7] D. Diakonov, L. M. Jensen, C. J. Pethick, and H. Smith, Physical Review A **66**, 013604 (2002).

[8] B. T. Seaman, L. D. Carr, and M. J. Holland, Physical Review A **72**, 033602 (2005).

[9] M. Machholm, C. J. Pethick, and H. Smith, Physical Review A **67**, 053613 (2003).

[10] B. Wu and Q. Niu, Physical Review A **61**, 023402 (2000).

[11] M. Jona-Lasinio, O. Morsch, M. Cristiani, N. Malossi, J. H. Müller, E. Courtade, M. Anderlini, and E. Arimondo, Physical Review Letters **91**, 230406 (2003).

[12] M. Machholm, A. Nicolin, C. J. Pethick, and H. Smith, Physical Review A **69**, 043604 (2004).

[13] V. M. Stojanović, C. J. Wu, W. V. Liu, and S. Das Sarma, Physical Review Letters **101**, 125301 (2008).

[14] C. J. Wu, Modern Physics Letters B **23**, 1 (2009).

[15] M. Ölschläger, G. Wirth, and A. Hemmerich, Physical Review Letters **106**, 15302 (2011).

[16] G. Wirth, M. Ölschläger, and A. Hemmerich, Nature Physics **7**, 147 (2011).

[17] T. Kock, M. Ölschläger, A. Ewerbeck, W.-M. Huang, L. Mathey, and A. Hemmerich, Physical Review Letters **114**, 1 (2015).

[18] A. J. Ferris, M. J. Davis, R. W. Geursen, P. B. Blakie, and A. C. Wilson, Physical Review A **77**, 012712 (2008).

[19] S. Burger, F. S. Cataliotti, C. Fort, F. Minardi, M. Inguscio, M. L. Chiofalo, and M. P. Tosi, Physical Review Letters **86**, 4447 (2001).

[20] B. Wu and Q. Niu, Physical Review A **64**, 061603 (2001).

[21] H.-Y. Hui, R. Barnett, J. V. Porto, and S. Das Sarma, Physical Review A **86**, 063636 (2012).

[22] E. Altman, A. Polkovnikov, E. Demler, B. I. Halperin, and M. D. Lukin, Physical Review Letters **95**, 20402 (2005).

[23] M. Anderlini, P. J. Lee, B. L. Brown, J. Sebby-Strabley, W. D. Phillips, and J. V. Porto, Nature **448**, 452 (2007).

[24] J. Sebby-Strabley, M. Anderlini, P. S. Jessen, and J. V. Porto, Physical Review A **73**, 033605 (2006).

[25] See appendix.

[26] O. Morsch, J. H. Müller, M. Cristiani, D. Ciampini, and E. Arimondo, Phys. Rev. Lett. **87**, 140402 (2001).

[27] A. Sinatra, C. Lobo, and Y. Castin, J. Phys. B **35**, 3599 (2002).

[28] C. Pethick and H. Smith, *Bose-Einstein Condensation in Dilute Gases* (Cambridge University Press, 2002).